Stick-slip phase transitions in confined solidlike films from an equilibrium perspective

Philippe Bordarier*
Laboratoire de Chimie-Physique des Matériaux Amorphes (URA 1104, CNRS), Bâtiment 490, Université de Paris-Sud, F-91405 Orsay, France

Martin Schoen†
Institut für Theoretische Physik, Sekretariat PN 7-1, Fachbereich Physik, Technische Universität Berlin, Hardenbergstraße 36, D-10623 Berlin, Germany
and Fachbereich Physik, Bergische Universität Wuppertal, Gaußstraße 20, D-42097 Wuppertal, Germany

Alain H. Fuchs‡
Laboratoire de Chimie-Physique des Matériaux Amorphes (URA 1104, CNRS), Bâtiment 490, Université de Paris-Sud, F-91405 Orsay, France

(Received 25 August 1997)

We investigate the transition from stick to slip conditions in sheared monolayer films confined between two plane parallel solid substrates. Each substrate consists of N_s atoms rigidly fixed in the (100) configuration of the face-centered cubic lattice. Shearing of the film is effected in a quasistatic (reversible) process in view of the low shear rates (on a molecular scale) in corresponding laboratory experiments employing the *surface forces apparatus* (SFA). To mimic operating conditions of the SFA as closely as possible we employ the grand isostress ensemble in which the temperature T, the chemical potential μ of the film, the stress T_{zz} exerted normally on the substrates, and the shear stress T_{zx} acting on the film in the x direction are among the thermodynamic state parameters. We analyze the average transverse alignment of the substrates (i.e., the registry) $\langle \alpha_x \ell \rangle$ (where ℓ is the lattice constant of the substrate) and its fluctuations $\xi^2 := \langle (\alpha_x \ell - \langle \alpha_x \ell \rangle)^2 \rangle$ in corresponding Monte Carlo simulations. Up to the so-called yield point $\langle \alpha_x^{\text{yield}} \ell \rangle$, $\langle \alpha_x \ell \rangle$ increases with T_{zx}; in the thermodynamic limit T_{zx} reaches its maximum at $\langle \alpha_x^{\text{yield}} \ell \rangle$ and $\xi^2 \to \infty$. For $\langle \alpha_x \ell \rangle \leqslant \langle \alpha_x^{\text{yield}} \ell \rangle$ the substrate ''sticks'' to the film; for $\langle \alpha_x \ell \rangle > \langle \alpha_x^{\text{yield}} \ell \rangle$ the substrate ''slips'' across the film's surface. States characterized by $\langle \alpha_x \ell \rangle > \langle \alpha_x^{\text{yield}} \ell \rangle$ are inaccessible in the grand isostress ensemble because they are thermodynamically unstable. Thus, the stick-slip phase transition occurs at $\langle \alpha_x^{\text{yield}} \ell \rangle$ in the thermodynamic limit. An analysis of the grand isostress potential indicates that stick-slip transitions can be viewed as continuous phase transitions where the yield point is an analog of the (liquid-gas) critical point. In a finite system the stick-slip phase transition occurs at rupture points $\langle \alpha_x^{\text{rupture}} \ell \rangle < \langle \alpha_x^{\text{yield}} \ell \rangle$ because ξ^2 may exceed a system-size-dependent free-energy barrier. [S1063-651X(98)01502-5]

PACS number(s): 61.20.Ja, 68.45.Nj

I. INTRODUCTION

The lifetime and durability of mechanical machines are often determined by friction between movable machine parts and wear. Lubricants consisting of, say, organic fluids can be employed to reduce the impact of these ultimately destructive phenomena. Their functioning depends to a large extent on the nature of the interaction between the fluid and the solid substrate it lubricates [1]. This is particularly so if the desire of engineers is to miniaturize certain machine parts [2]. In this case the lubricant may become a thin film of a thickness of only one or two molecular layers. The impact of such severe confinement is perhaps best illustrated by the dramatic increase of the shear viscosity in a hexadecane film of a thickness of two molecular layers, which may exceed the bulk shear viscosity by four orders of magnitude [3]. Understanding the rheological properties of such ultrathin, confined films is therefore of importance from a fundamental as well as from an applied technological perspective. Consequently, the rheological behavior of confined, molecularly thin films has been under intensive study in recent years, spurred by the development of a host of scanning probe devices such as the atomic force microscope (AFM) [4–8] and the surface forces apparatus (SFA) [9–13], which allow the study of such films directly on the nano or molecular scales.

In essence the SFA consists of two solid substrates traditionally covered with molecularly smooth mica sheets (walls) sandwiching the film of the fluid of interest. On a molecular length scale the mica sheets may be taken as plane parallel. The sandwich is immersed in the bulk fluid maintained at constant temperature and pressure. Thus, the film is *open* to the bulk reservoir, which serves as a thermal and material reservoir. Once thermodynamic equilibrium is established between the film and the reservoir, the temperature and the chemical potential of the film are fixed. By electromechanical means the separation and the transverse alignment between the walls can be manipulated with nearly molecular precision so that the confined film can be exposed to

*Electronic address: bordarie@cpma.u-psud.fr
†Electronic address: M.Schoen@physik.tu-berlin.de, schoen@wpta2.physik.uni-wuppertal.de
‡Electronic address: fuchs@cpma.u-psud.fr

compressional and shear strains, respectively.

In the latter case exposition to a shear strain is effected by attaching a movable stage to the upper wall via a spring characterized by its spring constant k [3,14,15] and moving this stage at some constant velocity in, say, the x direction parallel to the film-wall interface. Experimentally it is observed that the upper wall first ''sticks'' to the film as it were because the upper wall remains stationary. From the known spring constant and the measured elongation of the spring, the shear stress sustained by the film can be determined. Beyond a critical shear strain (i.e., at the so-called ''yield point,'' which corresponds to the maximum shear stress sustained by the film) the shear stress declines abruptly and the upper wall ''slips'' across the surface of the film. If the stage moves at a sufficiently low speed the walls eventually come to rest again until the critical shear stress is once again attained so that the stick-slip cycle repeats itself periodically.

This stick-slip cycle, observed for all types of film compounds ranging from long-chain (e.g., hexadecane) to spheroidal (e.g., octamethylcyclotetrasiloxane) hydrocarbons [12] has been attributed by Gee *et al.* [16] to the formation of solidlike films that pin the walls together (region of sticking) and must be made to flow plastically in order for the walls to slip. This suggests that the structure of the walls induces the formation of a solid film when the walls are properly registered and that this film ''melts'' when the walls are moved out of the correct registry. As first demonstrated in Ref. [17], such solid films may, in fact, form in ''simple''-fluid films between commensurate walls on account of a template effect imposed on the film by the discrete (i.e., atomically structured) walls. However, noting that the stick-slip phenomenon is general, in that it is observed in every liquid investigated, and that the yield stress may exhibit hysteresis, Granick [12] has argued that mere confinement may so slow mechanical relaxation of the film that flow must be activated on a time scale comparable with the experiment. This more general mechanism does not necessarily involve solid films, which can be formed only if the (solidlike) structure of the film and that of the walls possesses a minimum geometrical compatibility. In fact, it was recently demonstrated in a computer simulation study of a SFA model that formation of solid films is not a necessary prerequisite for the existence of a yield stress as observed experimentally [18]. Formation of solid films is prevented by walls whose structure is incommensurate with the solidlike structure the film would form under geometrically favorable conditions [18–20].

Theoretically many attempts have been made in recent years to elucidate details of stick-slip transitions observed in SFA experiments. The approaches can generally be grouped into two different categories, which may be labeled ''dynamical'' [21–27] and ''quasistatic'' [18,28–33]. In the dynamical approaches a stationary nonequilibrium state is created by either applying an external driving force [21] or by explicitly moving a substrate wall [22,24–27] in nonequilibrium molecular dynamics (NEMD) simulations in order to mimic dynamical aspects of a corresponding SFA experiment directly on a molecular scale. However, the relationship between NEMD simulations [22,24–27] and SFA experiments remains obscure for a number of reasons. First, in order to describe the motion of the substrate wall on a physical time scale, an equation of motion needs to be solved that inevitably involves the mass of the wall. However, there are no physical criteria on which the choice of a specific value for this mass could be based. Second, even though the wall is a macroscopic object in the SFA experiment, its mass cannot be too much larger than the mass of a film molecule in the NEMD simulations because otherwise the wall would remain at rest on the time scale on which film molecules move. In fact, the ratio of the mass of a single film molecule to that of the entire wall is sometimes as small as 1/8 [26,27] so that one can expect relaxation phenomena in the film to depend sensibly (and therefore unphysically from an experimental perspective) on this arbitrarily selected wall mass [28]. Third, the speed at which the walls are slid in the SFA experiment is typically of the order of 10^{-9}–10^{-7} Å ps^{-1} [12] so that under realistic conditions the walls remain practically stationary on a typical length and time scale of molecular relaxation processes. In NEMD simulations of SFA models one is therefore ineluctably forced to resort to unrealistically high shear rates (even if one assumes the film to be composed of molecules much heavier than rare gas atoms) in order to obtain a tractable signal-to-noise ratio for the quantities of interest so that the relevance of molecular-scale dynamical simulations to boundary lubrication phenomena remains highly questionable.

To avoid these problems and in view of the characteristic low shear rates in the actual SFA experiments we employ a ''quasistatic'' or reversible approach in which the thermodynamic state of the film passes through a succession of equilibrium states, each being distinguished by a different (average) lateral alignment of the walls [18,28–32]. Equilibrium properties of the film can be computed within the framework of Monte Carlo simulations carried out in various ensembles designed to capture key characteristics of a corresponding SFA experiment to a maximum degree. For example, in an SFA experiment one usually controls the stress applied normally to the wall (i.e., the load) and the shear stress(es). By making these variables parameters of a statistical physical ensemble it was demonstrated in Refs. [19,20,28] that details of the variation of the so-called solvation force with film thickness are in very good qualitative agreement with corresponding SFA experiments.

In this paper we apply the methodology developed in [19,20,28] to study stick-slip transitions in confined films under conditions of fixed normal and shear stresses. By fixing the shear strain rather than its conjugate stress [31,32] these investigations are complemented so that an interpretation of the stick-slip transition as a continuous phase transition emerges. Within the framework of this interpretation the yield point may be perceived as an analog of the critical point of a fluid. However, unlike the critical point the yield point is characterized by a divergence of fluctuations of the transverse alignment of the walls rather than a divergence of density fluctuations. While the stick-slip phase transition occurs at the yield point only in the thermodynamic limit, a pronounced system-size effect exists in the relatively small systems employed in computer simulations. Depending on the system size the stick-slip transition is shifted to so-called ''rupture points'' prior to the yield point. We will demonstrate that in a finite system a free energy (density) barrier exists between rupture and yield point that is related to a critical extent of registry fluctuations. The system remains

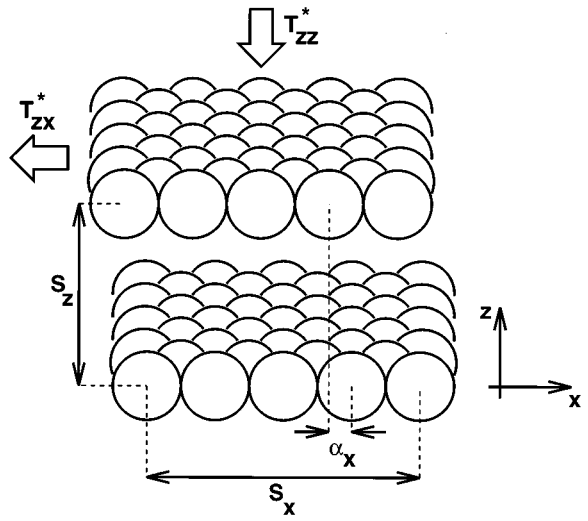

FIG. 1. Sketch of the model system where s_x and s_z are the side lengths of the lamella in the x and in the z directions, respectively (see Sec. III). The plane parallel, discrete walls are out of registry measured in terms of α_x so that the film between the walls (not shown) is exposed to a shear strain $\alpha_x\ell$ where ℓ is the lattice constant. In the configuration depicted the film is subjected to compressional (T_{zz}) and shear stresses (T_{zx}) indicated by arrows that point in arbitrarily chosen directions.

thermodynamically stable in the sticking regime if the registry fluctuations do not exceed the upper bound imposed by a generalized Gibbs free energy but undergoes a phase transition otherwise.

II. MODEL SYSTEM

Henceforth we focus on monolayer films consisting of an assembly of N molecules constrained between two solid substrates that are planar and parallel with each other along the z axis of the laboratory coordinate system (see Fig. 1). In general, each substrate consists of a number of planes of atoms parallel with the x-y plane. However, in this paper we take into account only the plane at the film-wall interface (i.e., the surface plane), consequently neglecting long-range film-wall interactions that result from interactions of film molecules with portions of the substrate below the surface plane [34]. These long-range film-wall interactions, which would be important for investigations of, say, wetting phenomena [35,36], are subdominant to the effect of mere confinement by the walls for the monolayer films of interest here [37,38]. Thus, we assume a single wall to consist of N_s atoms (wall atoms) distributed across the (z-directed) surface plane of area $A_z=s_xs_y$ according to the (100) configuration of the face-centered cubic (fcc) lattice where s_x and s_y denote the side lengths of the surface plane in the x and y direction, respectively. In these two directions the film is assumed infinite, which is effected by imposing periodic boundary conditions at the planes $x/s_x=\pm 0.5$ and $y/s_y=\pm 0.5$ so that the center of mass of the film coincides with the origin of the laboratory coordinate system located at $\mathbf{0}$. Since wall atoms are rigidly fixed, they are thermally decoupled from the film (i.e., the walls are maintained at a temperature $T=0$), which is a rather mild assumption in view of recent results for the shearing behavior of monolayer films between thermally coupled walls [39]. In the present model positions of wall atoms in both walls are related via

$$\begin{aligned} x_i^{[2]} &= x_i^{[1]} + \alpha_x \ell, \\ y_i^{[2]} &= y_i^{[1]}, \\ z_i^{[2]} &= z_i^{[1]} + s_z, \end{aligned} \tag{1}$$

where ℓ is the lattice constant, s_z is the distance between the walls along the z axis, and the registry $\alpha_x\ell$ specifies the relative lateral alignment of the walls in x. If $\alpha_x=\pm n$ ($n\in\mathbb{N}$) the walls are in registry; if $\alpha_x=\pm(n+1)/2$ they are out of registry. Superscripts in Eq. (1) refer to lower ($\{z_i^{[1]}\}=-s_z/2$) and upper wall ($\{z_i^{[2]}\}=+s_z/2$), respectively.

Interactions between film molecules and wall atoms as well as among film molecules are assumed to be pairwise additive. For simplicity we take film molecules to be spherically symmetric. The total configurational energy U of the system may be written as

$$\begin{aligned} U &= \sum_{i=1}^{N-1}\sum_{j=i+1}^{N} u(r_{ij}) + \sum_{k=1}^{2}\sum_{i=1}^{N}\sum_{j=1}^{N_s} u(r_{ij}^{[k]}) + \sum_{i=1}^{N} u_{hw}(z_i) \\ &=: U_{FF} + \sum_{k=1}^{2} U_{FW}^{[k]} + U_{HW}, \end{aligned} \tag{2}$$

where $r_{ij}:=|\boldsymbol{r}_i-\boldsymbol{r}_j|=[(x_i-x_j)^2+(y_i-y_j)^2+(z_i-z_j)^2]^{1/2}$ is the distance between the centers of mass of film molecules i and j located at $\boldsymbol{r}_i$ and $\boldsymbol{r}_j$, respectively. Likewise, $r_{ij}^{[k]}:=[(x_i-x_j^{[k]})^2+(y_i-y_j^{[k]})^2+(z_i-z_j^{[k]})^2]^{1/2}$ is the distance between film molecule i and wall atom j located in the lower ($k=1$) or in the upper ($k=2$) wall. In Eq. (2)

$$u_{hw}(z_i)=\begin{cases} 0, & |z_i|<s_z/2 \\ \infty, & |z_i|\geqslant s_z/2 \end{cases} \tag{3}$$

represents a hard-wall background potential introduced formally to prevent film molecules from escaping accidentally behind the surface plane. However, wall atoms are so densely packed that in practice film molecules do not interact with the hard-wall background during the course of a simulation on account of the strongly repulsive film-wall potential $u(r_{ij}^{[k]})$ at small distances $r_{ij}^{[k]}$. Equation (2) also defines the film-film (U_{FF}) and the film-wall contribution ($U_{FW}^{[k]}$) to the total configurational energy. In Eq. (2), $u(r)$ represents the Lennard-Jones(12,6) (LJ) potential, which we employ regardless of the nature of the interacting pair of particles [i.e., for film-film as well as for (continuous) film-wall interactions]. The LJ potential is given by

$$u(r)=4\epsilon\left[\left(\frac{\sigma}{r}\right)^{12}-\left(\frac{\sigma}{r}\right)^{6}\right], \tag{4}$$

where σ is the molecular ''diameter,'' ϵ is the well depth, and $r=r_{ij}$ or $r=r_{ij}^{[k]}$ depending on the nature of the interacting pair. For simplicity we take wall atoms and film molecules to be identical so that all interactions are governed by the same set of potential parameters $\{\epsilon,\sigma\}$.

III. STATISTICAL THERMODYNAMICS OF CONFINED FILMS IN THE GRAND ISOSTRESS AND ISOSTRAIN ENSEMBLES

A. Thermodynamics of strained films

Since we wish to describe shearing of the model films within the framework of a quasistatic approach, we need to summarize briefly the thermodynamics of confined molecularly thin films detailed in [40,41]. From a thermodynamic perspective it is generally necessary to distinguish between the *system* of interest and its *environment* and to specify the interaction between the two. In the present case we take as the system a finite lamella of the confined (infinite) film having dimensions $s_x \times s_y \times s_z$ [40,41]. The remainder of the film and the walls constitute the environment. The lamella can exchange compressional work with the environment by altering s_z or by changing the distances between the imaginary planes located at $x/s_x = \pm 0.5$ and $y/s_y = \pm 0.5$, which act like virtual ''pistons.''. In addition, the system can be exposed to a shear strain $\alpha_x\not{\ell}$ [see Eq. (1)]. The mechanical work due to infinitesimal compressional and shear strains can be expressed as

$$dW_{\mathrm{mech}} := -\sum_{\alpha} A_\alpha T_{\alpha\alpha} ds_\alpha - A_z T_{zx} d(\alpha_x\not{\ell}), \tag{5}$$

where $T_{\alpha\beta}$ is an element of the stress tensor and can be viewed as the average β component of the force applied normally to the area A_α pointing in the α direction ($\alpha = x,y,z$) [42,43]. Note that if the force exerted by the lamella on the α-directed face points outward, $T_{\alpha\beta}$ is negative by convention. Thus, dW_{mech} is the mechanical work done by the system on the environment. Diagonal and off-diagonal components of the stress tensor $\boldsymbol{T}$ are related to the work of compressing and shearing the lamella, respectively. Note that because the walls are rigid, they cannot be compressed or sheared, which is the reason for the absence of the four off-diagonal contributions involving T_{xz}, T_{yz}, T_{xy}, and T_{yx} in Eq. (5).

Gibbs' fundamental relation governing an infinitesimal, reversible transformation can be written as

$$dU = TdS + \mu dN - dW_{\mathrm{mech}}, \tag{6}$$

where U is the internal energy, T is the temperature, S is the entropy, and μ is the chemical potential. However, it is more convenient to express dW_{mech} in terms of A_z and the shape of the lamella $R := s_x/s_y$ [40,41]. In terms of these new variables

$$dU = TdS + \mu dN + \gamma' dA_z + \gamma'' A_z dR + T_{zz} A_z ds_z + T_{zx} A_z d(\alpha_x\not{\ell}), \tag{7}$$

where the interfacial tensions γ' and γ'' are related to combinations of the diagonal components of the stress tensor [40,41,44]. The third term on the right-hand side of Eq. (7) represents the work of changing the interfacial area A_z between the lamella and the wall whereas the fourth term is associated with the work done by the (rectangular) lamella as its shape R is changed at fixed area A_z.

To facilitate a description in terms of independent variables that can be controlled in actual laboratory experiments (i.e., T, μ, and the strains or their conjugate stresses), we introduce certain ancillary potentials via Legendre transformations. In particular, we will focus on

$$\Phi = U - TS - \mu N - T_{zz} A_z s_z \tag{8}$$

and

$$\hat{\Phi} = \Phi - T_{zx} A_z \alpha_x\not{\ell}. \tag{9}$$

The exact differentials of the thermodynamic potentials Φ and $\hat{\Phi}$ are obtained from Eqs. (8) and (9) with the help of Eq. (7) as

$$d\Phi(T,\mu,A_z,R,T_{zz},\alpha_x\not{\ell}) = -SdT - Nd\mu + \gamma' dA_z + \gamma'' A_z dR - A_z s_z dT_{zz} + T_{zx} A_z d(\alpha_x\not{\ell}) \tag{10}$$

and

$$d\hat{\Phi}(T,\mu,A_z,R,T_{zz},T_{zx}) = -SdT - Nd\mu + \hat{\gamma}' dA_z + \gamma'' A_z dR - A_z s_z dT_{zz} - A_z(\alpha_x\not{\ell}) dT_{zx}, \tag{11}$$

where

$$\hat{\gamma}' := \gamma' - T_{zx}\alpha_x\not{\ell}. \tag{12}$$

Since $\hat{\Phi}$ depends on the set of natural variables $\{T,\mu,A_z,R,T_{zz},T_{zx}\}$ it is most relevant to operating conditions of corresponding SFA experiments in which one controls directly T, μ, the compressional stress T_{zz}, and the shear stress T_{zx} [19,20,28].

B. Molecular description of confined strained films

The link between the macroscopic treatment summarized in Sec. III A and a molecular description is achieved via

$$\Phi(T,\mu,A_z,R,T_{zz},\alpha_x\not{\ell}) = -\beta^{-1} \ln \mathcal{Y}(T,\mu,A_z,R,T_{zz},\alpha_x\not{\ell}) \tag{13}$$

and

$$\hat{\Phi}(T,\mu,A_z,R,T_{zz},T_{zx}) = -\beta^{-1} \ln Y(T,\mu,A_z,R,T_{zz},T_{zx}) \tag{14}$$

established in Refs. [32] and [20], respectively. In Eqs. (13) and (14) $\beta := 1/k_B T$ (k_B is Boltzmann's constant) and

$$\mathcal{Y} := \sum_N \exp[\beta\mu N] \sum_{s_z} \exp[\beta T_{zz} A_z s_z] \times Q(N,T;A_z,R,s_z,\alpha_x\not{\ell}) = \left[\sum_{N,s_z} \cdots Q(N,T;A_z,R,s_z,\alpha_x\not{\ell})\right] \tag{15}$$

and

$$Y := \left[\sum_{N,s_z} \cdots \sum_{\alpha_x\not{\ell}} \exp[\beta T_{zx} A_z(\alpha_x\not{\ell})] \times Q(N,T;A_z,R,s_z,\alpha_x\not{\ell})\right] \tag{16}$$

are the partition functions of what shall henceforth be called a grand isostrain (thermodynamic potential Φ, partition function $\mathcal{Y}$) and a grand isostress ensemble (thermodynamic potential $\hat{\Phi}$, partition function Y) because both represent thermodynamically open systems but in the former a thermodynamic state is specified by fixing the shear strain $\alpha_x\ell$ as a natural parameter whereas the conjugate shear stress T_{zx} is a fixed state variable of the latter [45]. The shorthand notation $\Sigma_{N,s_z}\cdots$ introduced in Eq. (15) represents the double sum on N and s_z. In Eqs. (15) and (16) [46]

$$Q := \frac{Z_N}{N!\Lambda^{3N}} \tag{17}$$

is the canonical partition function in the classical limit for a system in which molecules possess only translational degrees of freedom, Λ is the thermal de Broglie wavelength [47], and

$$Z_N := \int_{V^N} d\boldsymbol{r}^N \exp[-\beta U(\boldsymbol{r}^N; A_z, R, s_z, \alpha_x\ell)] \tag{18}$$

is the configurational integral where the integration extends over the N-dimensional hypervolume V^N in configuration space.

Properties of interest in this work are the shear stress T_{zx}, its conjugate strain $\alpha_x\ell$, and fluctuations of these quantities. Molecular expressions for these quantities can be derived from Eqs. (10), (11), and (13)–(18). For example, from Eqs. (11), (14), and (16) it is straightforward to show that

$$\left(\frac{\partial\hat{\Phi}}{\partial T_{zx}}\right)_{T,\mu,A_z,R,T_{zz}} = -\beta^{-1}\left(\frac{\partial \ln Y}{\partial T_{zx}}\right)_{T,\mu,A_z,R,T_{zz}} = -(\beta Y)^{-1}\left[\sum_{N,s_z}\cdots\sum_{\alpha_x\ell}\beta A_z(\alpha_x\ell)\exp[\beta T_{zx}A_z(\alpha_x\ell)]\frac{Z_N}{N!\Lambda^{3N}}\right]$$
$$= -A_z\langle\alpha_x\ell\rangle, \tag{19}$$

where the angular brackets represent an ensemble average in the grand isostress ensemble. From Eq. (19) one verifies easily that

$$\left(\frac{\partial^2\hat{\Phi}}{\partial T_{zx}^2}\right)_{T,\mu,A_z,R,T_{zz}} = \beta^{-1}\left\{\left[\left(\frac{\partial \ln Y}{\partial T_{zx}}\right)_{T,\mu,A_z,R,T_{zz}}\right]^2 - Y^{-1}\left(\frac{\partial^2 Y}{\partial T_{zx}^2}\right)_{T,\mu,A_z,R,T_{zz}}\right\} = -\beta A_z[\langle(\alpha_x\ell)^2\rangle - \langle\alpha_x\ell\rangle^2]. \tag{20}$$

In a similar fashion one can derive a molecular expression for the shear stress T_{zx}. From Eqs. (10), (13), (15), (17), and (18) one obtains

$$A_z T_{zx} = \left(\frac{\partial\Phi}{\partial(\alpha_x\ell)}\right)_{T,\mu,A_z,R,T_{zz}} = -\beta^{-1}\left(\frac{\partial \ln \mathcal{Y}}{\partial(\alpha_x\ell)}\right)_{T,\mu,A_z,R,T_{zz}} = -(\beta\mathcal{Y})^{-1}\left(\sum_{N,s_z}\cdots\frac{1}{N!\Lambda^{3N}}\frac{\partial Z_N}{\partial(\alpha_x\ell)}\right). \tag{21}$$

The partial derivative of Z_N in Eq. (21) can be evaluated two ways leading to mathematically different but physically equivalent molecular expressions for T_{zx} that may be termed ''virial'' and ''force'' forms of T_{zx} [18,39]. In the present context the latter is more transparent. To derive it from Eq. (21) we rewrite Z_N in Eq. (18) as

$$Z_N = \prod_{i=1}^{N}\int_{-s_z/2}^{s_z/2}dz_i\int_{-s_y/2}^{s_y/2}dy_i\int_{\alpha_x\ell z_i/s_z-s_x/2}^{\alpha_x\ell z_i/s_z+s_x/2}dx_i\,\exp[-\beta U] =: \int_{\alpha_x\ell z_1/s_z-s_x/2}^{\alpha_x\ell z_1/s_z+s_x/2}dx_1 g_1(x_1) \tag{22}$$

defining an auxiliary quantity g_1 as

$$g_1(x_1) := \int_{-s_z/2}^{s_z/2}dz_1\int_{-s_y/2}^{s_y/2}dy_1\prod_{i=2}^{N}\int_{-s_z/2}^{s_z/2}dz_i\int_{-s_y/2}^{s_y/2}dy_i\int_{\alpha_x\ell z_i/s_z-s_x/2}^{\alpha_x\ell z_i/s_z+s_x/2}dx_i\,\exp[-\beta U]. \tag{23}$$

By applying Leibniz's rule for the differentiation of a parameter integral [48] one obtains

$$\frac{\partial Z_N}{\partial(\alpha_x\ell)} = \frac{z_1}{s_z}\underbrace{[g_1(x_1=\alpha_x\ell z_1/s_z+s_x/2)-g_1(x_1=\alpha_x\ell z_1/s_z-s_x/2)]}_{=0}$$
$$+\int_{\alpha_x\ell z_1/s_z-s_x/2}^{\alpha_x\ell z_1/s_z+s_x/2}dx_1\frac{\partial g_1(x_1)}{\partial(\alpha_x\ell)}\quad. \tag{24}$$

In Eq. (24) $U(x_1=\alpha_x\not{z}_1/s_z+s_x/2)=U(\alpha_x\not{z}_1/s_z-s_x/2)$ on account of periodic boundary conditions so that the first two terms on the right-hand side cancel out as indicated. Introducing now a new function g_2 defined analogously to g_1, the above argument may be repeated $N-1$ times, eventually yielding

$$\frac{\partial Z_N}{\partial(\alpha_x\not{z})}=-\beta\int_{V^N}d\boldsymbol{r}^N\frac{\partial U}{\partial(\alpha_x\not{z})}\exp[-\beta U(\boldsymbol{r}^N;A_z,R,s_z,\alpha_x\not{z})], \tag{25}$$

where U is given in Eq. (2). Because of Eq. (1) only $r_{ij}^{[2]}$ depends on $\alpha_x\not{z}$ so that Eq. (25) can be written more explicitly as

$$\begin{aligned}\frac{\partial Z_N}{\partial(\alpha_x\not{z})}&=-\beta\int_{V^N}d\boldsymbol{r}^N\frac{\partial U_{FW}^{[2]}}{\partial(\alpha_x\not{z})}\exp[-\beta U(\boldsymbol{r}^N;A_z,R,s_z,\alpha_x\not{z})]\\&=\beta\int_{V^N}d\boldsymbol{r}^N\exp[-\beta U(\boldsymbol{r}^N;A_z,R,s_z,\alpha_x\not{z})]\sum_{i=1}^{N}\sum_{j=1}^{N_s}u'(r_{ij}^{[2]})\frac{x_{ij}^{[2]}}{r_{ij}^{[2]}}\\&=-\beta\int_{V^N}d\boldsymbol{r}^N\exp[-\beta U(\boldsymbol{r}^N;A_z,R,s_z,\alpha_x\not{z})]F_x^{[2]},\end{aligned} \tag{26}$$

where $u'(r):=du/dr$, $x_{ij}^{[2]}:=x_i-x_j^{[2]}$, and $F_x^{[2]}$ is the x component of the force acting on the area A_z of the upper wall. Inserting Eq. (26) into Eq. (21) yields the desired force expression for the shear stress T_{zx}, namely,

$$A_zT_{zx}=\left(\frac{\partial\Phi}{\partial(\alpha_x\not{z})}\right)_{T,\mu,A_z,R,T_{zz}}=\langle F_x^{[2]}\rangle=-\langle F_x^{[1]}\rangle, \tag{27}$$

where the angular brackets now represent an ensemble average in the grand isostrain ensemble [cf. Eqs. (19) and (20)] and the far right hand side follows from the principle of mechanical stability.

Another quantity of interest is the shear modulus c_{44} (see Ref. [43] for notation) obtained by differentiating Eq. (27) according to

$$\begin{aligned}A_zc_{44}:&=\left(\frac{\partial^2\Phi}{\partial(\alpha_x\not{z})^2}\right)_{T,\mu,A_z,R,T_{zz}}=A_z\left(\frac{\partial T_{zx}}{\partial(\alpha_x\not{z})}\right)_{T,\mu,A_z,R,T_{zz}}\\&=-(\beta\mathcal{Y})^{-1}\left(\sum_{N,s_z}\cdots\frac{1}{N!\Lambda^{3N}}\frac{\partial^2Z_N}{\partial(\alpha_x\not{z})^2}\right)+\beta^{-1}\left[\mathcal{Y}^{-1}\left(\sum_{N,s_z}\cdots\frac{1}{N!\Lambda^{3N}}\frac{\partial Z_N}{\partial(\alpha_x\not{z})}\right)\right]^2,\end{aligned} \tag{28}$$

where the second line follows directly from Eq. (21). In the first term on the right-hand side of Eq. (28) we have

$$\frac{\partial^2Z_N}{\partial(\alpha_x\not{z})^2}=-\beta\int_{V^N}d\boldsymbol{r}^N\frac{\partial^2U_{FW}^{[2]}}{\partial(\alpha_x\not{z})^2}\exp[-\beta U]+\beta^2\int_{V^N}d\boldsymbol{r}^N\left(\frac{\partial U_{FW}^{[2]}}{\partial(\alpha_x\not{z})}\right)^2\exp[-\beta U], \tag{29}$$

where we invoked Eq. (26) and the same logic applies as before [see Eqs. (22)–(25)]. In Eq. (29) the partial derivative in the first integrand can be expressed more explicitly as

$$\frac{\partial^2U_{FW}^{[2]}}{\partial(\alpha_x\not{z})^2}=\frac{\partial}{\partial(\alpha_x\not{z})}\sum_{i=1}^{N}\sum_{j=1}^{N_s}u'(r_{ij}^{[2]})\frac{x_{ij}^{[2]}}{r_{ij}^{h[2]}}=-\sum_{i=1}^{N}\sum_{j=1}^{N_s}\left[u''\frac{x_{ij}^{[2]2}}{r_{ij}^{[2]2}}-\frac{u'}{r_{ij}^{[2]}}+u'\frac{x_{ij}^{[2]2}}{r_{ij}^{[2]3}}\right]. \tag{30}$$

Because of Eq. (26) the squared partial derivative of $U_{FW}^{[2]}$ in the second integral in Eq. (29) corresponds to $(F_x^{[2]})^2$ while the second term on the second line of Eq. (28) equals $\beta\langle F_x^{[2]}\rangle^2$ [see Eqs. (21) and (26)]. Thus, with these identifications one obtains from Eq. (28)

$$c_{44}=\underbrace{-\frac{\beta}{A_z}\left[\left\langle F_x^{[2]2}\right\rangle-\left\langle F_x^{[2]}\right\rangle^2\right]}_{<0}+\underbrace{\frac{1}{A_z}\left\langle\frac{\partial^2 U_{FW}^{[2]}}{\partial(\alpha_x\ell)^2}\right\rangle}_{>0}\gtrless 0 \tag{31}$$

where the positive contribution exceeds the negative one in magnitude up to the yield point [49]. Equation (31) shows that c_{44} is related to fluctuations of the x component of the force exerted by the lamella on the upper substrate and to the mean curvature [last term in Eq. (31)] of the lamella-wall configurational energy hyperplane. For symmetry reasons identically the same expression is obtained by replacing in Eq. (31) $U_{FW}^{[2]}$ by $U_{FW}^{[1]}$ and $F_x^{[2]}$ by $F_x^{[1]}$, respectively.

It is important to realize that c_{44} can also be computed in the grand isostress ensemble via

$$\begin{aligned}\left(\frac{\partial^2\Phi}{\partial(\alpha_x\ell)^2}\right)_{T,\mu,A_z,R,T_{zz}}&=A_z\left(\frac{\partial T_{zx}}{\partial(\alpha_x\ell)}\right)_{T,\mu,A_z,R,T_{zz}}\\&=\frac{A_z}{[\partial(\alpha_x\ell/\partial T_{zx})]_{T,\mu,A_z,R,T_{zz}}}\\&=-A_z^2\left(\frac{\partial^2\hat{\Phi}}{\partial(T_{zx})^2}\right)^{-1}_{T,\mu,A_z,R,T_{zz}},\end{aligned} \tag{32}$$

which follows directly from Eqs. (10) and (11). Employing Eq. (20), the definition of c_{44} given in Eq. (28), and Eqs. (31) and (32) can be used to arrive at

$$c_{44}=\frac{1}{\beta A_z[\langle(\alpha_x\ell)^2\rangle-\langle\alpha_x\ell\rangle^2]}=\frac{1}{\beta A_z\langle(\alpha_x\ell-\langle\alpha_x\ell\rangle)^2\rangle}\geqslant 0. \tag{33}$$

Equation (33) is one of the key results on which the present description of stick-slip transitions in confined films rests.

C. The grand isostress potential in the Gaussian limit

In the grand isostress ensemble the shear modulus can be related to the probability $P(\alpha_x\ell;\langle\alpha_x\ell\rangle)$ of finding a virtual system of this ensemble in a microstate characterized by a certain registry $\alpha_x\ell$. From Eq. (16) one realizes that

$$\begin{aligned}Y&=\sum_{\alpha_x\ell}\exp[\beta T_{zx}A_z\alpha_x\ell]\left[\sum_{N,s_z}\cdots Q(N,T)\right]\\&=:C^{-1}\sum_{\alpha_x\ell}P(\alpha_x\ell;\langle\alpha_x\ell\rangle),\end{aligned} \tag{34}$$

TABLE I. Second (μ_2) and fourth central moments (μ_4) of the probability $P(\alpha_x\ell;\langle\alpha_x\ell\rangle)$ obtained in grand isostress ensemble Monte Carlo simulations for different interfacial areas A_z and shear stresses T_{zx} at $T^*=1.00$, $\mu^*=-11.0$, and $T_{zz}^*=-1.00$. Also listed is the fourth-order cumulant U_4 [see Eq. (36)], which should vanish identically if $P(\alpha_x\ell;\langle\alpha_x\ell\rangle)$ is Gaussian (see text).

A_z^*	T_{zx}^*	$10^4\mu_2$	$10^7\mu_4$	U_4
63.880	0.00	4.314	5.622	−0.006
63.880	0.50	4.490	6.295	−0.041
63.880	1.00	4.917	7.507	−0.035
63.880	1.50	6.019	12.047	−0.108
63.880	1.60	6.485	14.354	−0.138
63.880	1.65 (rupture point)			
91.987	0.00	3.034	2.778	−0.006
91.987	0.50	3.069	2.804	0.007
91.987	1.00	3.392	3.505	−0.015
91.987	1.50	4.164	5.424	−0.043
91.987	1.60	4.492	6.628	−0.095
91.987	1.70	4.824	7.545	−0.081
91.987	1.80	5.388	10.826	−0.169
91.987	1.85 (rupture point)			
163.533	0.00	1.688	0.843	0.014
163.533	0.50	1.754	0.907	0.017
163.533	1.00	1.882	1.046	0.016
163.533	1.50	2.316	1.607	0.001
163.533	2.00	3.708	4.764	−0.155
163.533	2.05 (rupture point)			
255.520	0.50	1.115	0.363	0.026
255.520	1.00	1.199	0.428	0.007
255.520	2.00	2.197	1.442	0.003
255.520	2.10	2.856	2.854	−0.166
255.520	2.15 (rupture point)			

where C is a normalization constant. Expanding $\ln P$ in a Taylor series around $\langle\alpha_x\ell\rangle$ and truncating it after the quadratic term, a Gaussian approximation to P is obtained which can be expressed as

$$\begin{aligned}P(\alpha_x\ell;\langle\alpha_x\ell\rangle)=&\frac{1}{\sqrt{2\pi[\langle(\alpha_x\ell)^2\rangle-\langle\alpha_x\ell\rangle^2]}}\\&\times\exp\left\{-\frac{(\alpha_x\ell-\langle\alpha_x\ell\rangle)^2}{2[\langle(\alpha_x\ell)^2\rangle-\langle\alpha_x\ell\rangle^2]}\right\}\end{aligned} \tag{35}$$

after normalization such that $\int_{-\infty}^{\infty}d(\alpha_x\ell)P=1$. To establish the Gaussian character of $P(\alpha_x\ell;\langle\alpha_x\ell\rangle)$ under the present conditions, we computed $P(\alpha_x\ell;\langle\alpha_x\ell\rangle)$ as a histogram in grand isostress ensemble Monte Carlo simulations [19,20,28] (see Sec. III). A convenient measure of the Gaussian character of $P(\alpha_x\ell;\langle\alpha_x\ell\rangle)$ is the fourth-order cumulant defined as

$$U_4:=1-\frac{\mu_4}{3\mu_2^2}, \tag{36}$$

where

$$\mu_n := \int_{-\infty}^{\infty} d(\alpha_x \ell)(\alpha_x \ell - \langle \alpha_x \ell \rangle)^n P(\alpha_x \ell; \langle \alpha_x \ell \rangle), \quad n \in \mathbb{N} \tag{37}$$

is the nth central moment of $P(\alpha_x \ell; \langle \alpha_x \ell \rangle)$. For a Gaussian distribution $U_4 = 0$ because it is determined completely by μ_0 and μ_2, that is, all higher moments can be expressed in terms of the zeroth and second moments. Table I shows that for the numerically generated distributions $P(\alpha_x \ell; \langle \alpha_x \ell \rangle)$, $|U_4|$ is indeed small even for the largest stresses listed, which are very close to the values at which the stick-slip transition occurs in a finite system (see Sec. IV B). One notices that $|U_4|$ increases with T_{zx}, indicating that the Gaussian character is somewhat less well preserved for larger shear stresses. We note in passing that this points to the fact that, strictly speaking, the Gaussian approximation to $P(\alpha_x \ell; \langle \alpha_x \ell \rangle)$ becomes invalid at a (first- or second-order) phase transition because registry fluctuations are no longer small enough to justify the truncation of the Taylor-series expansion of $\ln P$ after the quadratic term [50]. However, keeping this in mind and because $|U_4|$ is still not too large even for the largest registries listed in Table I, we adopt the Gaussian form as a suitable lowest-level approximation to $P(\alpha_x \ell; \langle \alpha_x \ell \rangle)$ henceforth (see Sec. IV B).

In the present context another, particularly useful, representation of $P(\alpha_x \ell; \langle \alpha_x \ell \rangle)$ is obtained by inserting Eq. (33) into Eq. (35) so that

$$P(\alpha_x \ell; \langle \alpha_x \ell \rangle) = \sqrt{\frac{\beta A_z c_{44}(\langle \alpha_x \ell \rangle)}{2\pi}} \times \exp\left[-\frac{\beta(\alpha_x \ell - \langle \alpha_x \ell \rangle)^2 A_z c_{44}(\langle \alpha_x \ell \rangle)}{2} \right]. \tag{38}$$

In the thermodynamic limit ($A_z \to \infty$)

$$\lim_{A_z \to \infty} P(\alpha_x \ell; \langle \alpha_x \ell \rangle) = \delta(\alpha_x \ell - \langle \alpha_x \ell \rangle), \tag{39}$$

where δ denotes the Dirac δ function.

For later purposes we also wish to obtain an explicit expression for the grand isostress potential $\hat{\Phi}$ in terms of the average registry $\langle \alpha_x \ell \rangle$. From Eqs. (14) and (34) one obtains

$$\hat{\Phi} = -\beta^{-1} \ln\left(C^{-1} \sum_{\alpha_x \ell} P(\alpha_x \ell; \langle \alpha_x \ell \rangle) \right). \tag{40}$$

Differentiating this with respect to the shear stress T_{zx} gives

$$\left(\frac{\partial \hat{\Phi}}{\partial T_{zx}} \right)_{T,\mu,A_z,R,T_{zz}} = -A_z \langle \alpha_x \ell \rangle = \frac{d\hat{\Phi}}{d\langle \alpha_x \ell \rangle} \times \left(\frac{\partial \langle \alpha_x \ell \rangle}{\partial T_{zx}} \right)_{T,\mu,A_z,R,T_{zz}}, \tag{41}$$

where we have also invoked Eq. (19). The second factor on the far right-hand side of Eq. (41) is identified as c_{44}^{-1} through Eqs. (19), (20), and (33). Because of Eq. (38) one also has from Eq. (40)

$$\frac{d\hat{\Phi}}{d\langle \alpha_x \ell \rangle} = \beta^{-1} \frac{d \ln C}{d\langle \alpha_x \ell \rangle}. \tag{42}$$

Inserting Eq. (42) into Eq. (41) we obtain

$$d \ln C = -\beta A_z c_{44} d(\langle \alpha_x \ell \rangle), \tag{43}$$

which can be integrated provided an equation of state is known for $c_{44}(\langle \alpha_x \ell \rangle)$ so that $\hat{\Phi}$ is completely determined (see Sec. IV A).

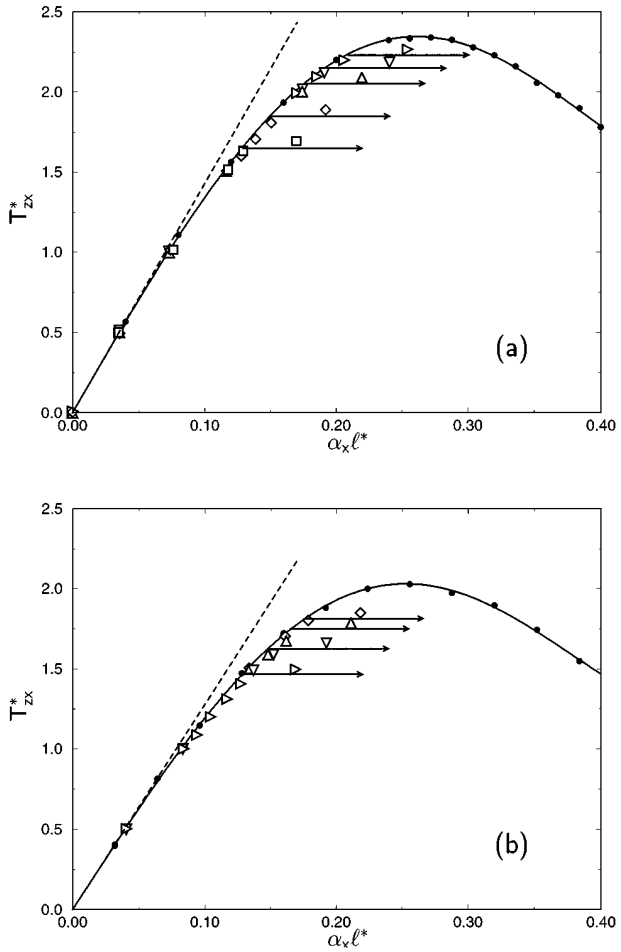

FIG. 2. The shear stress T^*_{zx} as a function of the shear strain $\alpha_x \ell^*$ for $T^* = 1.00$, $\mu^* = -11.00$. (a) $T^*_{zz} = -1.00$; (●): grand isostrain ensemble, open symbols represent grand isostress results for various areas $A^*_z = 63.880$ (□), 91.987 (◇), 163.533 (△), 255.520 (▽), and 574.921 (▷). The full curve is a fit to the grand isostrain-ensemble data intended to guide the eye. The dashed line corresponds to the Hookean limit (see text). The horizontal arrows indicate the shear stress at the rupture points (see text). (b) Same as (a), but for $T^*_{zz} = -0.50$; $A^*_z = 63.880$ (▷), 91.9876 (▽), 163.533 (△), 255.520 (◇).

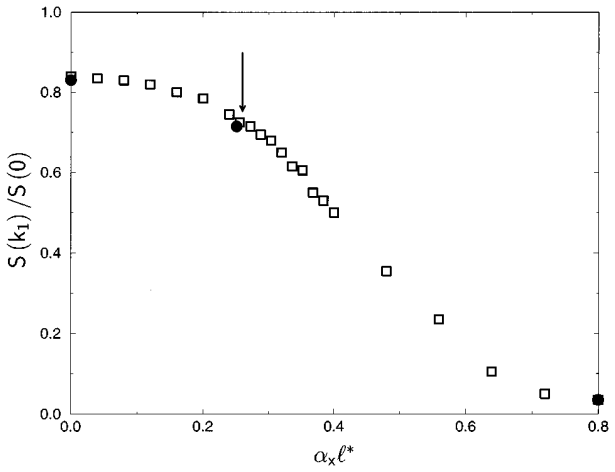

FIG. 3. The order parameter $S(k_1)/S(0)$ as a function of α from isostrain ensemble Monte Carlo simulations for $T^*=1.00$, $\mu^*=-11.00$, and $T_{zz}^*=-1.00$ (□) and $T_{zz}^*=-0.50$ (●). The arrow indicates the location of the yield point.

IV. RUPTURE AND YIELD POINTS

In the remainder of this paper all quantities will be given in the customary dimensionless (i.e., ''reduced'') units [51] indicated by an asterisk, that is energies will be given in units of ϵ, lengths in units of σ, and temperature in units of k_BT/ϵ. Thermodynamic states considered are exclusively based upon $T^*=1.00$ and $\mu^*=-11.00$ for which the LJ bulk phase is a moderately dense fluid characterized by a (average) number density $n^*:=\langle N\rangle/V^*=0.754$. Two states distinguished by $T_{zz}^*=-1.00$ and -0.50 are investigated. Because of $\ell^*=1.5985$ the walls are very slightly stretched, indicated by a distance $r^*=1.1303$ between nearest-neighbor wall atoms whereas the minimum of the LJ potential is at $r^*=2^{1/6}\simeq 1.1225$.

Furthermore, we note that the finite lamella of the infinite film introduced at the beginning of the preceding section is nothing but a virtual construct, entertained to comply with the principles of thermodynamics. In principle, the lamella can constitute any portion of the film. Thus, it is convenient to associate the lamella with the computational cell as far as the Monte Carlo simulations to be presented below are concerned. These simulations, carried out in the grand isostress and isostrain ensembles, employ algorithms fully described in Refs. [20,32]. The generation of a (numerical representation of a) Markov chain of configurations involves attempts to displace a film molecule at random, to insert a film molecule at a randomly selected point or to remove a randomly chosen film molecule, to change the separation between the walls [32], and, in the case of the grand isostress ensemble, to change the registry at random by a small amount [20] in addition to the three previous stochastic processes. Because attempts to change α_x affect all $2NN_s$ distances between film molecules and wall atoms and furthermore all N^2 distances between film molecules if s_z is altered, one needs to maintain the length of the relaxation period in systems of different sizes, that is for different interfacial areas A_z. This is achieved by fixing the relative frequency of these attempts according to $N{:}N{:}1(s_z)$ (grand isostrain ensemble) [32] and $N{:}N{:}1(s_z){:}1(\alpha_x)$ (grand isostress ensemble) [20].

A. Shear stress and shear modulus in the grand isostrain ensemble

In the grand isostrain ensemble the shear stress $T_{zx}(\alpha_x\ell)$ can be computed as an ensemble average via Eq. (27). Results for a monolayer film displayed in Fig. 2 show that $T_{zx}(\alpha_x\ell)$ vanishes for $\alpha_x\ell^*=0.0$ and 0.5 for symmetry reasons. For $\alpha_x=0.0$ the monolayer is solidlike regardless of the load (i.e., the value of T_{zz}). The solidlike structure is established from a plot of the order parameter $S(k_1)/S(0)$ [22] in Fig. 3 where the two-dimensional static structure factor is given by

$$S(\boldsymbol{k})=\frac{1}{N}\left|\sum_{j=1}^{N}\exp(i\boldsymbol{k}\cdot\boldsymbol{r}_j)\right|^2 \tag{44}$$

and $\boldsymbol{k}=(k_x,k_y,0)$. For a perfectly crystalline layer of film

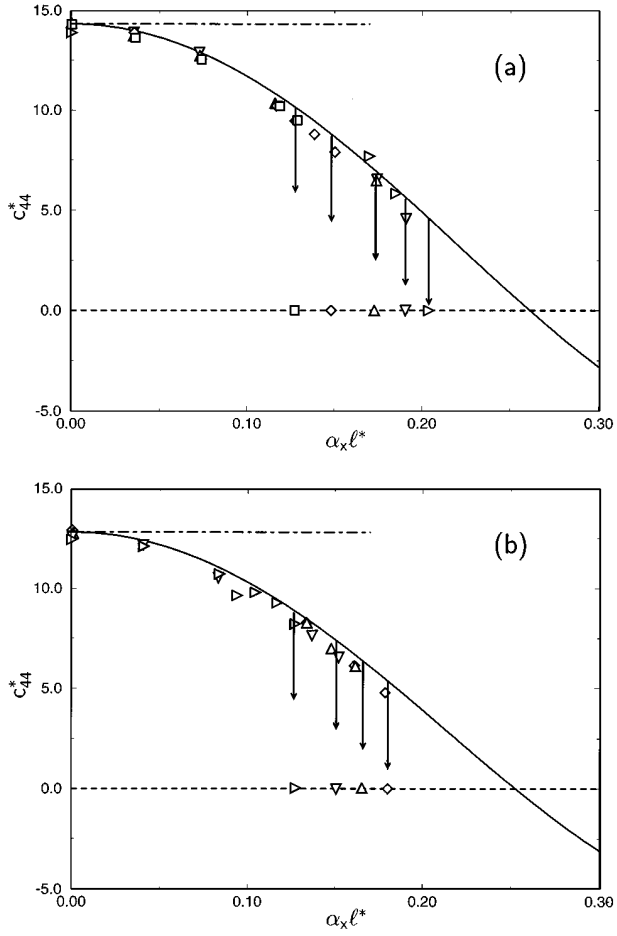

FIG. 4. The shear modulus c_{44}^* as a function of the shear strain $\alpha_x\ell^*$ for $T^*=1.00$, $\mu^*=-11.00$; (a) $T_{zz}^*=-1.00$, (b) $T_{zz}^*=-0.50$. The full line represents results obtained in the grand isostrain ensemble [see Eq. (31)]. Also shown are results obtained in the grand isostress ensemble for various areas A_z^* (see Fig. 2 for symbols). The vertical arrows indicate rupture-point locations for the various areas A_z. The yield point is located at the intersection between the full curve and the dashed horizontal line corresponding to $c_{44}^*=0$. The dashed-dotted horizontal line represents the Hookean limit in which $c_{44}=a_0$. Note that in the isostrain ensemble c_{44} may become negative for $\alpha_x\ell>\alpha_x^{\text{yield}}\ell$ (see text).

TABLE II. The set of fit parameters $\{a_0,a_2,a_4\}$ used to describe the dependence of c_{44} on the shear strain. The constant a_0 is a quantitative measure of rigidity of the film in the Hookean regime (i.e., $\alpha_x\ell \gtrsim 0.0$) [see Eq. (47)].

T^*	μ^*	T_{zz}^*	a_0^*	a_2^*	a_4^*
1.000	−11.00	−1.00	14.323	−271.382	901.840
1.000	−11.00	−0.50	12.805	−258.744	911.290

molecules at $T=0$ one expects the ratio $S(k_1)/S(0)=1$, where k_1 is the magnitude of the shortest reciprocal lattice vector [22]. Plots of the order parameter $S(k_1)/S(0)$ in Fig. 3 show that at $\alpha_x=0.0$ the monolayer films are indeed solidlike; the deviation of $S(k_1)/S(0)$ from its ideal value of 1.0 is due to thermal motion of film molecules. Thus, if the walls are in registry ($\alpha_x=\pm n, n\in\mathbb{N}$) they act like templates in the formation of a solidlike monolayer even though the corresponding bulk phase is still a liquid (see Sec. IV). As the film is progressively sheared, the degree of solidlike order diminishes but is still quite substantial at the yield point. At $\alpha_x=0.5$ the film is liquidlike as we infer from $S(k_1)/S(0)\simeq 0.0$. There is no significant dependence of the order parameter on T_{zz} so that apparently confinement effects are dominating the microscopic structure of the film in accord with earlier findings [37,38].

On the contrary, a comparison between Figs. 2(a) and 2(b) shows that the yield stress (the maximum value of T_{zx}) is about 15% higher for the larger load, indicating that a more stable film forms under higher loads. The greater rigidity of the film under higher loads is also reflected by its greater stiffness in the Hookean regime ($\alpha_x\ell \gtrsim 0$). A quantitative measure of the stiffness is the constant a_0 (see Table II), which is about 12% larger for the system exposed to the higher load. Thus, rheological properties of monolayer films are significantly influenced by the thermodynamic conditions. However, we note in passing that walls commensurate with the solidlike film are somewhat too idealized with respect to the SFA experiment (see Sec. I) [18,20,28]. The *qualitative* features and trends just discussed are, on the other hand, not altered greatly for severely confined films even if incommensurate walls are considered [18]. We do therefore not expect the present results to be qualitatively different if more realistic substrates are employed.

If exposed to a sufficiently small shear strain $\alpha_x\ell^* \gtrsim 0.0$, $T_{zx}(\alpha_x\ell)$ depends linearly on the strain according to Hooke's law [42] [see Figs. 2(a) and 2(b)]. However, as the strain increases further the film responds increasingly nonlinearly so that $T_{zx}(\alpha_x\ell)$ reaches a maximum, declines, and eventually vanishes at $\alpha_x=\pm(n+1)/2$ for symmetry reasons [18]. The maximum of the shear stress curve, which arises on account of the plastic response of the film to sufficiently high shear strains, determines the so-called yield point $\alpha_x^{\text{yield}}\ell$. Thermodynamic states for $\alpha_x\ell \leqslant \alpha_x^{\text{yield}}\ell$ are mechanically stable whereas these states become mechanically unstable if $\alpha_x\ell$ exceeds $\alpha_x^{\text{yield}}\ell$. Thus, for $\alpha_x\ell \leqslant \alpha_x^{\text{yield}}\ell$ the walls ''stick'' to the film while they can ''slip'' across the surface of the film for $\alpha_x\ell > \alpha_x^{\text{yield}}\ell$ so that the yield point separates the sticking from the slipping regime.

From the definition of the shear modulus c_{44} in Eq. (28) it is obvious that at the yield point

$$c_{44}(\alpha_x\ell)\big|_{\alpha_x\ell=\alpha_x^{\text{yield}}\ell}=0. \tag{45}$$

From this definition and the fact that the yield point represents a maximum of the shear stress curve it also follows that $c_{44}>0$ in the sticking regime ($\alpha_x\ell<\alpha_x^{\text{yield}}\ell$) and that $c_{44}<0$ in the slipping regime ($\alpha_x\ell>\alpha_x^{\text{yield}}\ell$), which can be verified directly from the plots in Fig. 4. For later purposes it is useful to represent the variation of the shear modulus with the shear strain by an equation of state. It can be obtained by expanding c_{44} in terms of higher-order elastic moduli of the unstrained solidlike film via

$$c_{44}(\alpha_x\ell)=c_{44}(0)+\frac{1}{2!}\left.\frac{\partial^2 c_{44}}{\partial(\alpha_x\ell)^2}\right|_{\alpha_x\ell=0}(\alpha_x\ell)^2+\frac{1}{4!}\left.\frac{\partial^2 c_{44}}{\partial(\alpha_x\ell)^2}\right|_{\alpha_x\ell=0}(\alpha_x\ell)^4+\cdots=\sum_{k=0}^{\infty}a_{2k}(\alpha_x\ell)^{2k}, \tag{46}$$

where a_0 corresponds to the shear modulus of a solidlike film in the Hookean limit ($\alpha_x\ell \gtrsim 0$) (see Figs. 2 and 4); coefficients $\{a_{2k}\}$ ($k>0$) can be viewed as higher-order elastic moduli of the unstrained solidlike film [33]. Molecular expressions for the higher-order elastic moduli can be derived in principle by differentiating c_{44} in Eq. (28) with respect to $\alpha_x\ell$. For the unstrained solidlike film odd derivatives $\partial^{(2k+1)}c_{44}(\alpha_x\ell)/\partial(\alpha_x\ell)^{(2k+1)}|_{\alpha_x\ell=0}$ vanish identically when averaged because they involve odd powers of $x_{ij}^{[2]}$ [see Eq. (30)]. Therefore, Eq. (46) involves only even powers of $\alpha_x\ell$. Even though the expansion coefficients could in principle be computed via their molecular expressions, these turn out to be far too complex to be evaluated numerically in grand isostrain ensemble Monte Carlo simulations [49]. It is therefore more sensible to obtain the set $\{a_{2k}\}$ by fitting the polynomial in Eq. (46) to $c_{44}(\alpha_x\ell)$ over a certain range of shear strains. In practice an excellent representation of $c_{44}(\alpha_x\ell)$ is obtained by truncating the sum in Eq. (46) after the third term [33], which yields

$$c_{44}=a_0+a_2(\alpha_x\ell)^2+a_4(\alpha_x\ell)^4+O[(\alpha_x\ell)^6]. \tag{47}$$

Plots in Fig. 4 show that in the Hookean regime ($\alpha_x\ell \gtrsim 0$) $c_{44}\simeq$ const, declines steadily with increasing $\alpha_x\ell$ up to the yield point at which by definition $c_{44}=0$ [see Eq. (45)], and becomes negative at larger shear strains. The smaller c_{44} the more pronounced is the nonlinear, plastic response of the film to an applied shear strain. It is particularly noteworthy that the representation of c_{44} is excellent even for states be-

yond the yield point that are mechanically unstable because $c_{44}<0$ [33]. Values for the set $\{a_0,a_2,a_4\}$ are listed in Table II for the thermodynamic states considered here.

B. Rupture points and finite-size effects

In the grand isostress ensemble, on the other hand, c_{44} is positive semidefinite and therefore cannot become negative according to Eq. (33). Consequently, thermodynamic states characterized by $\langle\alpha_x\rangle\geqslant\langle\alpha_x^{\rm yield}\rangle$ are inaccessible. Since $c_{44}=0$ at the yield point one expects registry fluctuations to diverge at this point according to Eq. (33). The restriction $c_{44}(\langle\alpha_x\rangle)\geqslant 0$ in the grand isostress ensemble as compared to the grand isostrain ensemble is akin to the one encountered in studies of liquid-gas phase equilibria employing, say, the canonical and grand canonical ensembles. Because the density is fixed in the former, thermodynamic states pertaining to the two-phase liquid-gas regime are accessible even though these states are *mechanically* unstable, that is, for these states the isothermal compressibility $\kappa_T:=-1/V(\partial V/\partial P)<0$ in a finite system where P is the bulk pressure and V is the volume. In the grand canonical ensemble, on the other hand, the constraint of fixed n is lifted so that this ensemble has one additional degree of freedom. One can then prove that κ_T is positive definite and consequently thermodynamic states in the liquid-gas two-phase region become inaccessible because of their *thermodynamic* instability [46].

The same can be said with regard to the relation between grand isostress and isostrain ensembles where the former has one additional degree of freedom compared with the latter because the registry is not fixed [see Eqs. (15) and (16)]. Thus, it is tempting to perceive the average registry $\langle\alpha_x\rangle$ as the analog of the average density n in the grand canonical ensemble and to view $c_{44}^{-1}\propto\langle(\alpha_x)^2\rangle-\langle\alpha_x\rangle^2$ [see Eq. (33)] as the analog of $\kappa_T\propto\langle N^2\rangle-\langle N\rangle^2$ [46] in this ensemble. This notion is supported further by noting that $\langle\alpha_x\rangle$ and c_{44}^{-1} in Eq. (33) are related to first and second derivatives of $\hat{\Phi}$ with respect to T_{zx} [see Eqs. (19) and (20)] just like n and κ_T are related to first and second derivatives of the grand potential Ω with respect to μ [37]. In this spirit and within the framework of the quasistatic description of the SFA experiment it seems fruitful to regard the transition from stick to slip conditions at the yield point as a continuous phase transition because $(\partial\hat{\Phi}/\partial T_{zx})_{T,\mu,A_z,R,T_{zz}}\propto\langle\alpha_x^{\rm yield}\rangle$ remains finite and $(\partial^2\hat{\Phi}/\partial T_{zx}^2)_{T,\mu,A_z,R,T_{zz}}\rightarrow\infty$ [see Eqs. (19), (20), (33), Figs. 2, and 4].

However, an inspection of Figs. 2 and 4 shows that the system in the grand isostress ensemble undergoes a transition from stick to slip conditions prior to the yield point as reflected by a divergence of the registry fluctuations at so-called ''rupture points'' characterized by $\langle\alpha_x^{\rm rupture}\rangle<\langle\alpha_x^{\rm yield}\rangle$. We emphasize that up to the rupture point Eq. (47) provides a good representation of $c_{44}(\langle\alpha_x\rangle)$ in the grand isostress ensemble with the same set of values for $\{a_0,a_2,a_4\}$ obtained by fitting Eq. (47) to $c_{44}(\alpha_x)$ in the grand isostrain ensemble (see Fig. 4). Thus,

$$c_{44}(\langle\alpha_x\rangle)=c_{44}(\alpha_x)\quad\forall\langle\alpha_x\rangle\leqslant\langle\alpha_x^{\rm rupture}\rangle. \tag{48}$$

Closer scrutiny seems to reveal a small but systematic trend of c_{44} obtained in the grand isostress ensemble to be smaller than its grand isostrain counterpart. However, given an estimated 5% for the mutual error bars on both data sets these deviations are considered insignificant.

The origin of the rupture points may be rationalized as follows. If $\langle\alpha_x\rangle$ is close enough to the yield point there is a nonvanishing probability $P(\alpha_x;\langle\alpha_x\rangle)>0$ for registries to exceed $\langle\alpha_x^{\rm yield}\rangle$ *on average*. These states are *in principle* inaccessible in the grand isostress ensemble because c_{44} would be negative which is precluded on account of Eq. (33). One therefore expects any finite film to become thermodynamically unstable at $\langle\alpha_x^{\rm rupture}\rangle$ prior to the yield point if the probability for registries exceeding the yield point is nonzero. In the actual grand isostress ensemble Monte Carlo simulations 0.5–2% of all configurations generated at $\langle\alpha_x^{\rm rupture}\rangle$ are characterized by registries exceeding $\langle\alpha_x^{\rm yield}\rangle$ under the present conditions. Consequently the film undergoes a transition from stick to slip conditions earlier than at $\langle\alpha_x^{\rm yield}\rangle$. For shear stresses in the interval $T_{zx}^{\rm rupture}\leqslant T_{zx}\leqslant T_{zx}^{\rm yield}$ (where $T_{zx}^{\rm rupture}$ and $T_{zx}^{\rm yield}$ correspond to the shear stresses at rupture and yield points, respectively) one observes a persistent increase of the lateral displacement of the upper substrate wall as a function of the Monte Carlo ''time.'' This displacement is irregular in that it is characterized by short periods of variable length over which the upper substrate remains stationary alternating with periods of motion. Similar effects have been reported experimentally for squalane films, which were, however, sheared in real time [52].

One also notices from Table I a general trend of μ_2 and μ_4 to decrease with increasing A_z at fixed T_{zx} even for registries for which the value of $|U_4|$ is quite small so that the Gaussian approximation to $P(\alpha_x;\langle\alpha_x\rangle)$ is still well justified. The decrease of the central moments indicates that $P(\alpha_x;\langle\alpha_x\rangle)$ becomes increasingly peaked around $\langle\alpha_x\rangle$. In other words, registry fluctuations decrease with A_z [see Eqs. (35) and (39)]. At the same time the location of the rupture point shifts towards the yield point as A_z becomes larger, i.e., as $P(\alpha_x;\langle\alpha_x\rangle)$ becomes more peaked at $\langle\alpha_x\rangle$. However, for any finite interfacial area A_z there will always be a finite spread of $P(\alpha_x;\langle\alpha_x\rangle)$ around $\langle\alpha_x\rangle$. Because of the diminishing extent of registry fluctuations [i.e., the increasing sharpness of $P(\alpha_x;\langle\alpha_x\rangle)$] with increasing interfacial area one expects $\langle\alpha_x^{\rm rupture}\rangle=f(A_z)$, a conjecture confirmed by the plots in Fig. 5. However, one notes from Fig. 5 a fairly weak dependence of $\langle\alpha_x^{\rm rupture}\rangle$ on the thermodynamic state.

Furthermore, in the thermodynamic limit $\lim_{A_z\rightarrow\infty}\langle\alpha_x^{\rm rupture}\rangle=\langle\alpha_x^{\rm yield}\rangle$ should hold because of Eq. (39) (see Fig. 5). Based on this logic and the previous observations it seems plausible to introduce a ''rupture length'' ξ_r,

$$\xi_r(T,\mu,A_z,R,T_{zz},T_{zx})\geqslant\sqrt{\langle(\alpha_x)^2\rangle-\langle\alpha_x\rangle^2}, \tag{49}$$

as a measure of an upper limit for registry fluctuations where the equal sign holds at the rupture point. Because of Eq. (33), Eq. (49) implies

$$c_{44}\geqslant\frac{1}{\beta A_z\xi_r^2}, \tag{50}$$

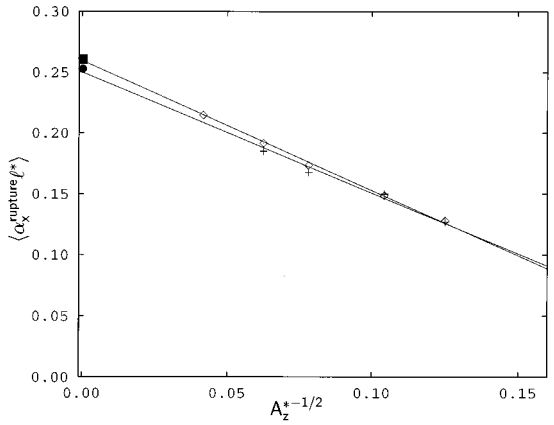

FIG. 5. The rupture-point location $\langle \alpha_x^{\text{rupture}} \not{\ell} \rangle$ as a function of $A_z^{-1/2}$ for $T^*=1.00$, $\mu^*=-11.00$, $T_{zz}^*=-1.00$ ($\diamond$), and $T_{zz}^*=-0.50$ ($+$). The straight lines represent fits of the empirical scaling law [see Eq. (55)] (see text). Yield-point locations from corresponding grand isostrain ensemble Monte Carlo simulations [(■), $T_{zz}^*=-1.00$; (●), $T_{zz}^*=-0.50$] agree well with the extrapolated ($A_z^{*-1/2}=0$) grand isostress ensemble data; only grand isostress ensemble data were included in the fit.

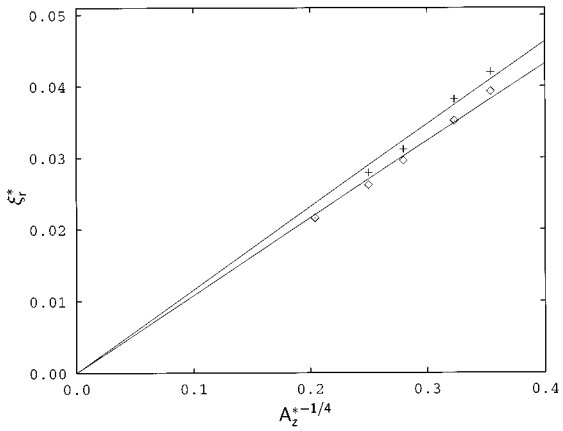

FIG. 6. The rupture length ξ_r^* as a function of $A_z^{*-1/4}$ [see Eq. (57)] for $T^*=1.00$, $\mu^*=-11.00$, $T_{zz}^*=-1.00$ ($\diamond$), and $T_{zz}^*=-0.50$ ($+$). The straight line is calculated from Eq. (57) using $\{a_2, a_4\}$ from Table II and $\{a, \langle \alpha_x^{\text{yield}} \not{\ell}^* \rangle\}$ from the fit of Eq. (55) to the simulation data shown in Fig. 5 (see text).

where again the equal sign applies at the rupture point. Equation (50) states that in any finite film the degree of plasticity (reflected by the value of c_{44}) must not exceed a certain (system-size dependent) critical value for the film to remain thermodynamically stable in the sticking regime. The degree of plasticity may be cast quantitatively as

$$\frac{dc_{44}}{d\langle \alpha_x \not{\ell} \rangle}\Big|_{\langle \alpha_x \not{\ell} \rangle = \langle \alpha_x^{\text{yield}} \not{\ell} \rangle} = 2a_2 \langle \alpha_x \not{\ell} \rangle + 4a_4 \langle \alpha_x \not{\ell} \rangle^3 < 0, \tag{51}$$

that is, by the deviation of $c_{44}(\langle \alpha_x \not{\ell} \rangle)$ from Hookean behavior defined by

$$\frac{dc_{44}}{d\langle \alpha_x \not{\ell} \rangle} = 0 \quad \forall \langle \alpha_x \not{\ell} \rangle. \tag{52}$$

Note that a Hookean film has no yield point because $c_{44}=a_0>0$ [see Eq. (47)] and that registry fluctuations cannot diverge because of

$$\beta A_z c_{44} = \beta A_z a_0 = \frac{1}{\langle (\alpha_x \not{\ell})^2 \rangle - \langle \alpha_x \not{\ell} \rangle^2} \neq 0. \tag{53}$$

Equation (53) shows that for a Hookean film a yield point does not exist (infinite-system limit). Thus, a solidlike Hookean film cannot be liquified by applying a shear strain. Employing once again the analogy between yield and (liquid-gas) critical points advocated here, a Hookean film may be viewed as an idealization in the spirit of the ideal-gas model.

To estimate the rupture length we employ Eqs. (47) and (50) and get

$$\xi_r = \{\beta A_z [a_0 + a_2 \langle \alpha_x^{\text{rupture}} \not{\ell} \rangle^2 + a_4 \langle \alpha_x^{\text{rupture}} \not{\ell} \rangle^4]\}^{-1/2}. \tag{54}$$

Results plotted in Fig. 6 indicate that ξ_r decreases with increasing A_z as expected. The dependence of ξ_r on the thermodynamic state is again weak because the rupture-point location itself is found to depend only marginally on the precise nature of the state (see Fig. 5). Comparison with Fig. 5 shows that the rupture-point location shifts towards the yield point over the same range of interfacial areas as it should. We emphasize that the yield-point location can be calculated directly in the grand isostrain ensemble from either $\max_{\alpha_x \not{\ell}} T_{zx}(\alpha_x \not{\ell})$ or $c_{44}(\alpha_x \not{\ell})=0$ (see Figs. 2 and 4). Thus, the reliability of the rupture-point location obtained in the grand isostress ensemble can be verified by extrapolation of $\langle \alpha_x^{\text{rupture}} \not{\ell} \rangle$ to the thermodynamic limit ($A_z \to \infty$) where $\langle \alpha_x^{\text{rupture}} \not{\ell} \rangle = \langle \alpha_x^{\text{yield}} \not{\ell} \rangle$ according to the foregoing reasoning (see Sec. IV C).

C. Scaling behavior

Because of the pronounced system-size dependence of both $\langle \alpha_x^{\text{rupture}} \not{\ell} \rangle$ and ξ_r it is instructive to investigate the scaling behavior of both quantities with A_z. This is facilitated by plotting $\langle \alpha_x^{\text{rupture}} \not{\ell} \rangle$ as a function of $1/\sqrt{A_z}$ in Fig. 5, which gives a nearly perfect representation of the Monte Carlo data regardless of the thermodynamic state of the film. Note that in Fig. 5 the yield-point $\langle \alpha_x^{\text{yield}} \not{\ell} \rangle$ obtained by fitting

$$\langle \alpha_x^{\text{rupture}} \not{\ell} \rangle = \langle \alpha_x^{\text{yield}} \not{\ell} \rangle + \frac{a}{\sqrt{A_z}}, \quad a<0 \tag{55}$$

to the simulation data (taking $\langle \alpha_x^{\text{yield}} \not{\ell} \rangle$ and a as fit parameters) in a least-squares fashion agrees very well with $\alpha_x^{\text{yield}} \not{\ell}$ determined independently in a corresponding grand isostrain ensemble Monte Carlo simulation under the same thermodynamic conditions. The empirical scaling law for $\langle \alpha_x^{\text{rupture}} \not{\ell} \rangle$ given in Eq. (55) may be employed in Eq. (47) to express c_{44} at the rupture point in terms of A_z and the parameter a. Noting that $c_{44}(\langle \alpha_x^{\text{yield}} \not{\ell} \rangle)=0$ one obtains the scaling relation

$$c_{44}(\langle \alpha_x^{\text{rupture}} \rangle) = a \left. \frac{dc_{44}}{d\langle \alpha_x \rangle} \right|_{\langle \alpha_x \rangle = \langle \alpha_x^{\text{yield}} \rangle} A_z^{-1/2} + O(A_z^{-1}) \tag{56}$$

in a macroscopic system (i.e., as $A_z \to \infty$), which is again determined by the degree of plasticity [see Eq. (51)]. Since the rupture-point location coincides with the yield point according to Eq. (55) in the thermodynamic limit, it is not surprising that c_{44} vanishes as $A_z \to \infty$. One therefore expects the rupture length to vanish in that limit too. From Eqs. (54) and (56) one obtains the scaling relation for the rupture length as

$$\begin{aligned} \xi_r &= \left[\beta a \left. \frac{dc_{44}}{d\langle \alpha_x \rangle} \right|_{\langle \alpha_x \rangle = \langle \alpha_x^{\text{yield}} \rangle} \right]^{-1/2} [A_z^{1/2} + O(A_z^0)]^{-1/2} \\ &\simeq \left[\beta a \left. \frac{dc_{44}}{d\langle \alpha_x \rangle} \right|_{\langle \alpha_x \rangle = \langle \alpha_x^{\text{yield}} \rangle} \right]^{-1/2} A_z^{-1/4}, \end{aligned} \tag{57}$$

which is confirmed by the plot in Fig. 6. In other words, the critical registry fluctuations at the rupture point are related to the degree of plasticity at the yield point. It is furthermore noteworthy from the plot that the dependence of ξ_r on the interfacial area is in accord with the scaling law despite the relative smallness of the simulation cells employed.

Another interesting observation can be made from the scaling law in Eq. (56) with respect to the values of the thermodynamic potential at yield and rupture points, respectively. This can be demonstrated by integrating Eq. (43) with the aid of Eq. (47) and inserting the resulting expression into Eq. (40). Based upon the Gaussian approximation for $P(\alpha_x; \langle \alpha_x \rangle)$ (which should be valid only approximately at the rupture point, see Sec. III B) one eventually arrives at

$$\hat{\Phi} = A_z \left(\frac{a_0}{2} \langle \alpha_x \rangle^2 + \frac{a_2}{4} \langle \alpha_x \rangle^4 + \frac{a_4}{6} \langle \alpha_x \rangle^6 \right) \geqslant 0, \tag{58}$$

which is a physically sensible expression because $\hat{\Phi} = 0$ for the unsheared solidlike film and because $\hat{\Phi}$ increases the more the film is exposed to a shear stress. This follows from Eqs. (47) and (58) because of

$$\begin{aligned} \frac{d\hat{\Phi}}{d\langle \alpha_x \rangle} &= A_z \langle \alpha_x \rangle (a_0 + a_2 \langle \alpha_x \rangle^2 + a_4 \langle \alpha_x \rangle^4) \\ &= A_z \langle \alpha_x \rangle c_{44}(\langle \alpha_x \rangle) \geqslant 0 \quad \forall \langle \alpha_x \rangle \leqslant \langle \alpha_x^{\text{yield}} \rangle. \end{aligned} \tag{59}$$

However, it is more convenient to turn to the corresponding (generalized Gibbs) free energy density rather than employing the thermodynamic potential $\hat{\Phi}$ itself. Therefore, we introduce $\tilde{\hat{\Phi}} := A_z^{-1} \hat{\Phi}$, which is an intensive quantity. Let us now compute $\tilde{\hat{\Phi}}(\langle \alpha_x^{\text{rupture}} \rangle)$ including only terms up to the order of $O(A_z^{-1/2})$. From Eqs. (55) and (58) we obtain

$$\begin{aligned} \Delta\tilde{\hat{\Phi}} &:= \tilde{\hat{\Phi}}_{\text{yield}} - \tilde{\hat{\Phi}}_{\text{rupture}} \simeq -a A_z^{-1/2} c_{44}(\langle \alpha_x^{\text{rupture}} \rangle) = -\frac{a}{\beta A_z^{3/2} [\langle (\alpha_x^{\text{rupture}})^2 \rangle - \langle \alpha_x^{\text{rupture}} \rangle^2]} \\ &= -a\beta^{-1} A_z^{-3/2} \frac{1}{\xi_r^2} \simeq -a^2 \langle \alpha_x^{\text{yield}} \rangle \left. \frac{dc_{44}}{d\langle \alpha_x \rangle} \right|_{\langle \alpha_x \rangle = \langle \alpha_x^{\text{yield}} \rangle} A_z^{-1} \geqslant 0, \end{aligned} \tag{60}$$

which is the generalized Gibbs free-energy density barrier for the stick-slip transition at the rupture point for a system with finite interfacial area. Equation (60) shows that the free energy density barrier depends on the degree of plasticity defined in Eq. (51) of the sheared film at the yield point. Because of Eq. (33) this is equivalent to saying that $\Delta\tilde{\hat{\Phi}}$ is determined by the rupture length, that is by the critical registry fluctuations at the rupture point. The generalized Gibbs free-energy density as defined here is positive semidefinite because c_{44} in the grand isostress ensemble is positive semidefinite [see Eq. (33)]. This implies $a < 0$ (A_z finite) because $\langle \alpha_x^{\text{yield}} \rangle$ is the largest possible (average) registry in this ensemble. The generalized Gibbs free-energy density barrier depends on the thermodynamic state through a, a_2, a_4 [see Eq. (51)], and the yield point location. To undergo a transition from stick to slip conditions the system has to overcome $\Delta\tilde{\hat{\Phi}}$, which decreases with increasing interfacial area. Because of Eq. (58) the generalized Gibbs free-energy density $\tilde{\hat{\Phi}} < \tilde{\hat{\Phi}}_{\text{rupture}} \forall \langle \alpha_x \rangle < \langle \alpha_x^{\text{rupture}} \rangle$ so that the threshold value $\Delta\tilde{\hat{\Phi}}$ is approached from above. Thus, because $\langle \alpha_x \rangle = f(T_{zx})$ is a monotonically increasing function (see Figs. 2 and 4) (and therefore $\tilde{\hat{\Phi}}$ is a monotonically decreasing function) of T_{zx} the film has to be exposed to a sufficiently large shear stress before this transition can take place. This critical stress increases with A_z but cannot exceed the yield stress because $\Delta\tilde{\hat{\Phi}}$ is positive semidefinite.

V. DISCUSSION AND CONCLUSIONS

In this article we investigated the transition from stick to slip conditions in monolayer films under shear composed of

spherically symmetric film molecules that are confined between discretely structured, commensurate walls. Shearing is effected under conditions closely resembling those of corresponding SFA experiments in that the normal load on the walls is maintained in the simulations as well as the temperature and the chemical potential of the film. Since in an SFA experiment one usually controls the shear stress acting on the film, we employ the grand isostress ensemble in which the stress tensor component T_{zx} is a natural parameter of the relevant thermodynamical potential. From a theoretical perspective it is instructive to supplement these calculations by employing a corresponding grand isostrain ensemble in which the relative transverse alignment of the walls is controlled rather than the conjugate shear stress T_{zx}. Our main results can be summarized as follows.

(1) The shear modulus can be expressed rigorously in terms of registry fluctuations, indicating that c_{44} is positive semidefinite [see Eq. (33)]. From this it follows that in the grand isostress ensemble thermodynamic states become unstable if the (average) registry $\langle \alpha_x \rangle$ exceeds that of the yield point defined by $c_{44}(\langle \alpha_x^{\text{yield}} \rangle)=0$. At the yield point registry fluctuations diverge because the shear modulus vanishes. Up to the yield point registry fluctuations increase steadily and monotonically because c_{44} is a smooth, nonsingular function of $\langle \alpha_x \rangle$ (see Figs. 2 and 4).

(2) In the thermodynamic limit ($A_z \to \infty$) a transition from stick to slip conditions will therefore occur at the yield point where c_{44}^{-1} is singular so that the stick-slip transition may legitimately be viewed as a phase transition in the thermodynamic sense.

(3) In a finite system ($A_z < \infty$) the stick-slip phase transition is subject to a finite-size effect so that the transition occurs at rupture points prior to the yield point (see Figs. 2 and 4). The rupture-point location depends on the film-wall interfacial area and follows a simple empirically established scaling law $\langle \alpha_x^{\text{rupture}} \rangle \propto A_z^{-1/2}$ (see Fig. 5) so that in the thermodynamic limit the locations of rupture and yield points coincide.

(4) In a finite system a transition from stick to slip conditions occurs at a rupture point because there is a nonvanishing probability for the registry to exceed $\langle \alpha_x^{\text{yield}} \rangle$ on average due to nonvanishing registry fluctuations. For registries above the yield point c_{44} would be negative which is precluded in the grand isostress ensemble on account of Eq. (33). Consequently, these fluctuations have to be limited if the system is to remain in the sticking regime. By introducing the concept of a rupture length ξ_r [see Eq. (49)] we observe a relative root mean square fluctuation of the registry $\xi_r / \langle \alpha_x^{\text{rupture}} \rangle$ of about $8-15\%$ depending on the interfacial area. Despite the relative smallness of the simulation cell $\xi_r \propto A_z^{-1/4}$ as one would expect for a macroscopic system (see Fig. 6).

(5) Stick-slip phase transitions are not *driven* by shear-induced melting of the confined film (see Fig. 3).

That shear-induced melting does not *drive* the stick-slip transition is in accordance with earlier investigations in which the shear melting point is located through characteristic maxima in the heat capacity, the compressibility, and the expansion coefficient of the film and is found to occur only at registries significantly above the yield point [53]. One also knows that film molecules do not diffuse on the typical time scales of a fluid for all registries up to and significantly above the yield point [54]. From the perspective of the grand isostress ensemble the film would therefore have to become thermodynamically unstable *prior* to melting. However, it should be noted that *after* the stick-slip phase transition has occurred (i.e., when the registry diverges) the film will lose its solidlike structure accompanied by drainage, thus rapidly becoming disordered and therefore liquidlike. In this sense the stick-slip transition is the *cause* of shear-induced melting of the film and triggers it contrary to what was surmised in Ref. [22].

The earlier studies [18,30,32,33,39,53] also show that shearing is a continuous process. This notion is once again confirmed here, reflected in particular by the continuous variation of the shear modulus with the shear stress in the grand isostress ensemble. Because of this one also expects the grand isostress potential to be a continuous function up to and at the yield point because in an infinite system $c_{44}=0$ is thermodynamically permissible. This implies, however, that the first derivative of the grand isostress potential [see Eq. (19)] remains finite at the yield point but that the second derivative, related to c_{44}^{-1}, diverges, which is the ''fingerprint'' of a continuous phase transition.

Perhaps the most prominent continuous phase transition occurs at the critical point of a fluid at which density fluctuations diverge while the density n itself remains finite. Based upon the analogy $\langle \alpha_x^{\text{yield}} \rangle \Leftrightarrow n$ and $c_{44}^{-1} \Leftrightarrow \kappa_T$ advocated in Sec. IV B it is tempting to associate the stick-slip phase transition with a novel, shear-stress driven critical phenomenon. From this angle the yield point is the associated critical point. In fact, it has been argued [55] that stick-slip transitions may arise on account of self-organized criticality if a material is exposed to a sufficiently large shear stress (or strain), a concept that has been applied recently to friction phenomena [56]. Consequently, the rupture point has to be viewed as a shear-critical point shifted on account of the (artificial) finiteness of the system. The rupture length ξ_r is a quantitative measure of this shift, vanishing only in the thermodynamic limit.

ACKNOWLEDGMENTS

We acknowledge helpful discussions with Steve Granick (University of Illinois) and thank Siegfried Hess (Technische Universität Berlin) and Dennis J. Diestler (University of Nebraska–Lincoln) for reading the manuscript. P.B. and M.S. acknowledge financial support from the Sonderforschungsbereich 335 ''Anisotrope Fluide.'' M.S. is grateful to the Deutsche Forschungsgemeinschaft for financial support.

[1] B. Bhushan, J. N. Israelachvili, and U. Landman, Nature (London) **374**, 607 (1995).
[2] T. A. Core, W. K. Tsang, and S. J. Sherman, Solid State Technol. **36**, 39 (1993).
[3] J. Van Alsten and S. Granick, Phys. Rev. Lett. **61**, 2570 (1988).
[4] G. Binnig, C. F. Quate, and C. Gerber, Phys. Rev. Lett. **56**, 930 (1986).
[5] C. M. Mate, G. M. McClelland, R. Erlandsson, and S. Chiang, Phys. Rev. Lett. **59**, 1942 (1987).
[6] R. Erlandsson, G. Hadziioannou, C. M. Mate, G. M. McClelland, and S. Chiang, J. Chem. Phys. **89**, 5190 (1989).
[7] E. Meyer, Prog. Surf. Sci. **41**, 3 (1992).
[8] M. B. Salmeron, MRS Bull. **18**, 20 (1993).
[9] D. Tabor and R. H. S. Winterton, Proc. R. Soc. London, Ser. A **312**, 435 (1969).
[10] J. N. Israelachvili and D. Tabor, Proc. R. Soc. London, Ser. A **331**, 19 (1973).
[11] J. N. Israelachvili and P. M. McGuiggan, Science **241**, 795 (1989).
[12] S. Granick, Science **253**, 1374 (1991).
[13] G. Reiter, A. L. Demirel, J. Peanasky, L. L. Cai, and S. Granick, J. Chem. Phys. **101**, 2606 (1994).
[14] J. N. Israelachvili, P. M. McGuiggan, and A. M. Homola, Science **240**, 189 (1988).
[15] J. Israelachvili, P. McGuiggan, M. Gee, A. Homola, M. Robbins, and P. Thompson, J. Phys.: Condens. Matter **2**, SA89 (1990).
[16] M. L. Gee, P. M. McGuiggan, J. N. Israelachvili, and A. M. Homola, J. Chem. Phys. **93**, 1895 (1990).
[17] M. Schoen, D. J. Diestler, and J. H. Cushman, J. Chem. Phys. **87**, 5464 (1987).
[18] M. Schoen, S. Hess, and D. J. Diestler, Phys. Rev. E **52**, 2587 (1995).
[19] P. Bordarier, B. Rousseau, and A. H. Fuchs, Mol. Simul. **17**, 199 (1996).
[20] P. Bordarier, B. Rousseau, and A. H. Fuchs, J. Chem. Phys. **106**, 7295 (1997).
[21] B. N. J. Persson, Phys. Rev. B **48**, 18 140 (1993).
[22] P. A. Thompson and M. O. Robbins, Science **250**, 792 (1990).
[23] P. A. Thompson and M. O. Robbins, Phys. Rev. A **41**, 6830 (1990).
[24] M. Lupkowski and F. van Swol, J. Chem. Phys. **95**, 1995 (1991).
[25] P. A. Thompson, G. S. Grest, and M. O. Robbins, Phys. Rev. Lett. **68**, 3448 (1992).
[26] M. G. Rozman, M. Urbakh, and J. Klafter, Phys. Rev. Lett. **77**, 683 (1996).
[27] M. G. Rozman, M. Urbakh, and J. Klafter, Phys. Rev. E **54**, 6485 (1996).
[28] P. Bordarier, Dissertation, Université de Paris-Sud, 1997.
[29] M. Schoen, C. L. Rhykerd, Jr., D. J. Diestler, and J. H. Cushman, Science **245**, 1223 (1989).
[30] M. Schoen, D. J. Diestler, and J. H. Cushman, Phys. Rev. B **47**, 5603 (1993).
[31] D. J. Diestler, M. Schoen, and J. H. Cushman, Science **262**, 545 (1993).
[32] M. Schoen, D. J. Diestler, and J. H. Cushman, J. Chem. Phys. **100**, 7707 (1994).
[33] M. Schoen, Mol. Simul. **17**, 369 (1996).
[34] W. A. Steele, *The Interaction of Gases with Solid Surfaces* (Pergamon Press, Oxford, 1974).
[35] S. Dietrich, in *Phase Transitions and Critical Phenomena*, edited by C. Domb and J. L. Lebowitz (Academic, London, 1988), Vol. 12.
[36] M. Schick, in *Liquides aux Interfaces*, Les Houches 1988 Session XLVIII, Course Nine, edited by J. Charvolin, J. Joanny, and J. Zinn-Justin (North-Holland, Amsterdam, 1990).
[37] M. Schoen, Ber. Bunsenges. Phys. Chem. **100**, 1355 (1996).
[38] M. Schoen, J. Chem. Phys. **105**, 2910 (1996).
[39] M. Schoen, Physica A **240**, 328 (1997).
[40] D. J. Diestler, M. Schoen, J. E. Curry, and J. H. Cushman, J. Chem. Phys. **100**, 9140 (1994).
[41] D. J. Diestler and M. Schoen, Acta Chim. Hungar. — Models in Chemistry **132**, 45 (1995).
[42] L. D. Landau and E. M. Lifschitz, *Lehrbuch der Theoretischen Physik* (Akademie-Verlag, Berlin, 1965), Vol. VII, Chap. 1.
[43] H. B. Callen, *Thermodynamics* (Wiley, New York, 1960), Chap. 13.
[44] D. J. Diestler, J. Phys. Chem. **100**, 10 414 (1996).
[45] The reader should note that the grand isostrain ensemble of this work was termed grand isostress ensemble in Ref. [32]; the grand isostress ensemble used here was termed grand isoforce in Ref. [20]. Different notation is used here for internal consistency and clarity.
[46] D. A. McQuarrie, *Statistical Mechanics* (Harper&Row, New York, 1976).
[47] J. P. Hansen and I. R. McDonald, *Theory of Simple Liquids*, 2nd ed. (Academic, London, 1986).
[48] G. Arfken, *Mathematical Methods for Physicists* (Academic, London, 1985), p. 478.
[49] M. Schoen (unpublished).
[50] L. D. Landau and E. M. Lifshitz, *Statistical Physics* (Pergamon, Oxford, 1958).
[51] M. P. Allen and D. J. Tildesley, *Computer Simulation of Liquids* (Clarendon, Oxford, 1987).
[52] A. L. Demirel and S. Granick, Phys. Rev. Lett. **77**, 4330 (1996).
[53] M. Schoen, D. J. Diestler, and J. H. Cushman, Mol. Phys. **78**, 1097 (1993).
[54] M. Schoen, J. H. Cushman, and D. J. Diestler, Mol. Phys. **81**, 475 (1994).
[55] P. Bak, C. Tang, and K. Wiesenfeld, Phys. Rev. Lett. **59**, 381 (1987).
[56] F. J. Elmer, in *Physics of Sliding Friction*, edited by B. N. J. Persson and E. Tossatti (Kluwer, Dordrecht, 1996), pp. 433–447.